Arch. Mech., 32, 5, pp. 675–685, Warszawa 1980

Investigations of the incompressible flow around an oscillating ellipsoid

W. GEISSLER and K. KIENAPPEL (GÖTTINGEN)

FOR THE DETAILED investigation of the unsteady flow about oscillating blunt bodies a sophisticated theoretical approach based on potential theory (panel method) as well as experimental data obtained in a low speed wind tunnel should help to get some insight into the complicated 3d-unsteady flow phenomena involved. A short description of the theoretical approach and of the test set-up are given. Comparisons between calculated and measured steady and unsteady surface pressure distributions are discussed in detail. Conclusions can be drawn from these results with respect to the different effects of viscosity of the flow about blunt bodies leading to different types of separation.

Dla szczegółowej analizy przepływów nieustalonych wokół drgających ciał zatępionych należy stosować dość wyrafinowane podejście teoretyczne oparte na teorii potencjału, jak również wyniki doświadczalne uzyskane w wolnoprzepływowym tunelu aerodynamicznym; metody te pozwalają uzyskać pewne informacje o złożonych zjawiskach związanych z trójwymiarowym przepływem nieustalonym. Podano w pracy krótki opis koncepcji teoretycznej oraz odpowiedniej aparatury badawczej. Przedyskutowano i porównano ze sobą obliczone teoretycznie i zmierzone wartości ustalonych i nieustalonych rozkładów ciśnień powierzchniowych. Z otrzymanych wyników wysnuć można wnioski dotyczące różnych efektów lepkości przy opływie ciał prowadzących do różnych typów oderwania.

Для детального анализа неустановившихся течений, вокруг затупленных колеблющихся тел, следует применять довольно тонкие теоретические подходы, опирающиеся на теорию потенциала, как тоже на экспериментальные результаты, полученные в аэродинамическом туннеле малых скоростей; эти методы позволяют получить некоторые сведения о сложных явлениях, связанных с трехмерным неустановившимся течением. В работе дается краткое описание теоретического подхода и соответсвующей исследовательской аппаратуры. Обсуждены и сравнены между собой расчитанные теоретически и измеренные значения установившихся и неустановившихся распределений поверхностных давлений. Из полученных результатов можно сделать выводы, касающиеся разных эффектов вязкости при обтекании тел, приводящие к разным типам отрыва.

1. Introduction

FOR THE PREDICTION of unsteady airloads on oscillating bodies a number of potential theoretical methods have been developed (for instance [1]) using linearized boundary conditions and the Bernoulli equation. The simplest approach is the well-known slender body theory. Due to the linearizations a complete separation of the problem into a steady and an unsteady part is achieved. But due to these simplifications two effects cannot be accounted for in an accurate manner:

1. Increasing bluntness of the body.
2. Three-dimensional effects in the case of an axis-symmetrical body at incidence.

Therefore a new method has been developed [2] which accounts for these effects and which is an exact solution of the governing Laplace equation together with the correspond-

ing unsteady boundary conditions and the Bernoulli equation. In the present investigation this method is proved by comparisons with experimental data obtained in the 3m-low speed wind tunnel of the DFVLR in Göttingen on an oscillating blunt ellipsoid of revolution with axis ratio $a/b = 3$.

These comparisons between the exact potential theory and the experimental data should clarify also the limits of potential theory on the one side and give some insight into the viscous effects occurring in the real flow on the other side.

These latter effects due to viscosity are expressed in the different types of separation occurring on such blunt bodies at incidence.

2. Potential-theoretical approach

For the limiting case of incompressible flow the governing potential equation reduces to the simple Laplace equation for which a Green function exists. This function can be interpreted as source-sink singularities which are placed on the real body surface. For the problem of an oscillating body in a parallel main flow, it is of advantage to use a body-fixed frame of reference. In such a system two different time-dependent velocity vectors can be specified.

2.1. Velocity vector due to the uncoming flow

For an observer on the oscillating body the uncoming parallel flow $\mathbf{U}_\infty$ changes its incidence in time with respect to the body axis, i.e. the x-axis (Fig. 1).

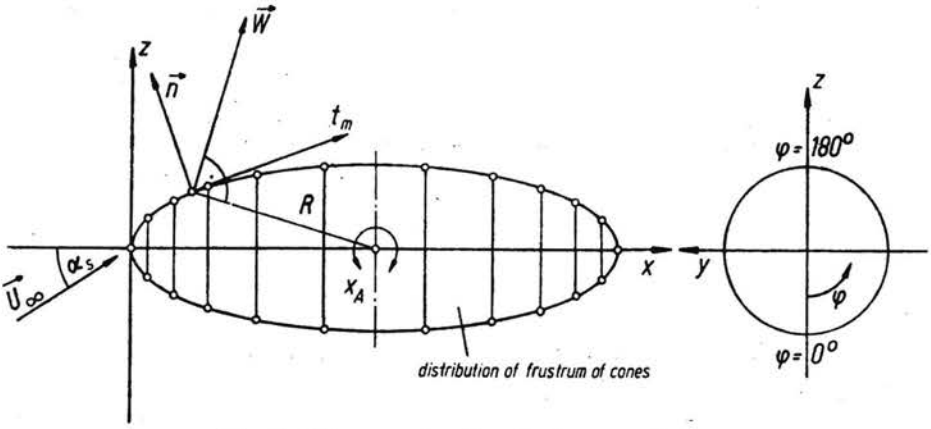

FIG. 1. Body geometry, discretization procedure.

Thus the instantaneous angle of incidence is

$$\alpha_t = \alpha_s + \alpha' e^{i\omega t} \tag{2.1}$$

with α_s as the steady mean incidence and α' as the amplitude of oscillation. ω is the angular frequency and t the time. In body-fixed coordinates the uncoming flow vector $\mathbf{U}_\infty$ can now be expressed in time-dependent x, y, z components by

$$
\begin{aligned}
U_{\infty x} &= U_\infty \cos \alpha_t, \\
U_{\infty y} &= 0 \\
U_{\infty z} &= U_\infty \sin \alpha_t.
\end{aligned} \tag{2.2}
$$

Rearranging the sin- and cos-terms in Eqs.(2.2) and making a series expansion of the resulting unsteady terms in powers of the oscillation amplitude α', the components in Eq. (2.2) can be expressed by a sum of a steady plus unsteady terms, the latter proportional to α', α'^2 etc. In most applications the higher order terms in α'^2 are negligible (small amplitude oscillations) and for the present discussions only this first order term is retained. It is shown, however [2], that it is possible to take into account also higher order terms without difficulties.

2.2. Velocity vector due to body oscillations

Figure 1 shows for the case of pitching oscillations about a pitching axis at $x = x_A$ that the velocity vector **W** due to the oscillatory movement of the body can easily be specified in arbitrary surface points. Important is the perpendicular distance R of the point from the axis of rotation. The velocity vector **W** is proportional to α'.

Adding steady and unsteady terms of $\mathbf{U}_\infty$ and **W**, one can now determine the prescribed normal components of these vectors in arbitrary surface points.

The problem is then treated by solving a Fredholm integral equation of the second kind: The strengths of a continuous singularity distribution on the body surface are determined such that the prescribed normal velocities are cancelled by the induced normal velocities of the sources and sinks:

$$
\frac{\partial \Phi}{\partial n} = -\mathbf{n}(\mathbf{U}_\infty + \mathbf{W}). \tag{2.3}
$$

The final numerical solution is done by a panel-type method. The body surface is split into small surface elements, each with a constant singularity strength. The determination of the source-sink strengths then leads to a large system of linear algebraic equations which can be solved by standard methods.

With the calculated singularity strengths it is then possible to specify steady and unsteady pressures using the time-dependent Bernoulli equation.

In the present method the case of axi-symmetric bodies has been handled in a more economic way. Due to the axis-symmetry the circumferential dependency of all flow parameters, i.e. velocities, singularity strengths etc. can be expressed by simple sin- and cos-expressions. Thus the integration of the aerodynamic influence functions in the φ-direction can be done analytically leading to complete elliptic integrals of the first and second kind. The body surface must therefore only be split up in axial direction into a frustums of cones of small axial dimensions (Fig. 1). The advantage of this modification is the possibility of taking a large number of surface elements without exceeding the storage of the computer. For the given results the surface of the body in axial direction is split into as much as 150 surface points with a concentration at the front and rear part of the body. Therefore very accurate results also for cases of moderate steady incidences with sharp pressure peaks have been achieved.

3. Test requirements

3.1. Test set-up

Figure 2 shows the model of the ellipsoid in the open test section of the 3m-low speed wind tunnel in Göttingen. For later investigation on a half-ellipsoid with cylindrical

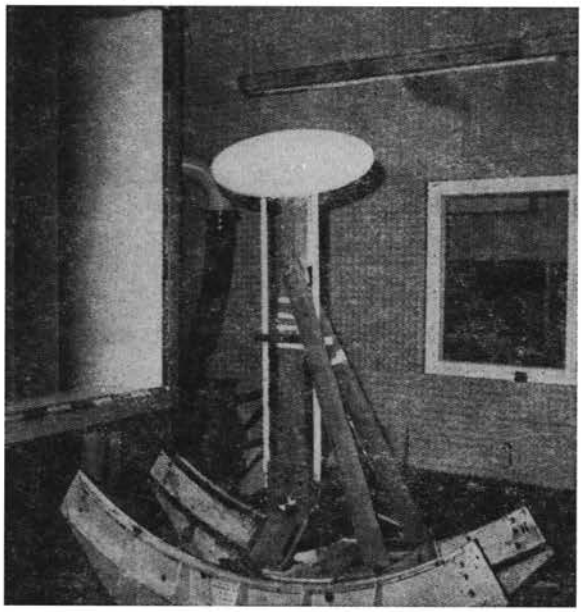

FIG. 2. Ellipsoid in the open test section of the 3m-low speed wind tunnel of the DFVLR Göttingen. Test set-up.

afterbody, the ellipsoid was build up by two half parts. The model was suspended vertically on a streamlined sting and excited to pitching oscillations about the midchord-axis by a hydraulic actuator fixed on the bottom of the model test rig. The oscillatory movement was transferred to the ellipsoid by two draw-bars. In addition to the oscillatory movement of the ellipsoid, the steady incidence could vary in the range of $+30° \geqslant \alpha_s \geqslant -15°$. In Fig. 3 we can see that the influence of the sting should be small with a minimum disturbance at the rear part of the body.

The model was equipped with a large number of pressure measuring taps located in the plane of symmetry ($\varphi = 0°/180°$) (Fig. 1) of the body as well as in three different circumferential planes at $x/L = 0.089; 0.196; 0.543$.

3.2. Measuring techniques

A block diagram of the measuring equipment is shown in Fig. 4. The movement of the body was controlled in a closed circuit by the signal of an angular displacement transducer.

Most of the pressure measuring taps are connected to the pressure transducers by tube-scanning valve systems (indirect method). The transfer functions of these systems

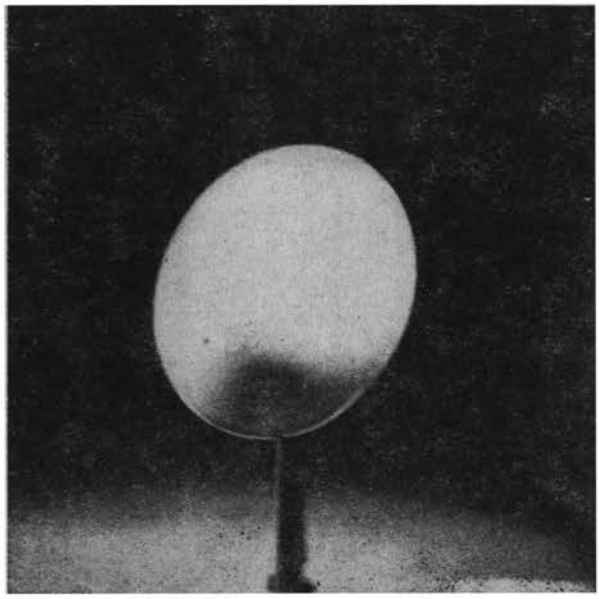

FIG. 3. Ellipsoid in the open test section of the 3m-low speed wind tunnel of the DFVLR Göttingen. Undisturbed rear part of the ellipsoid.

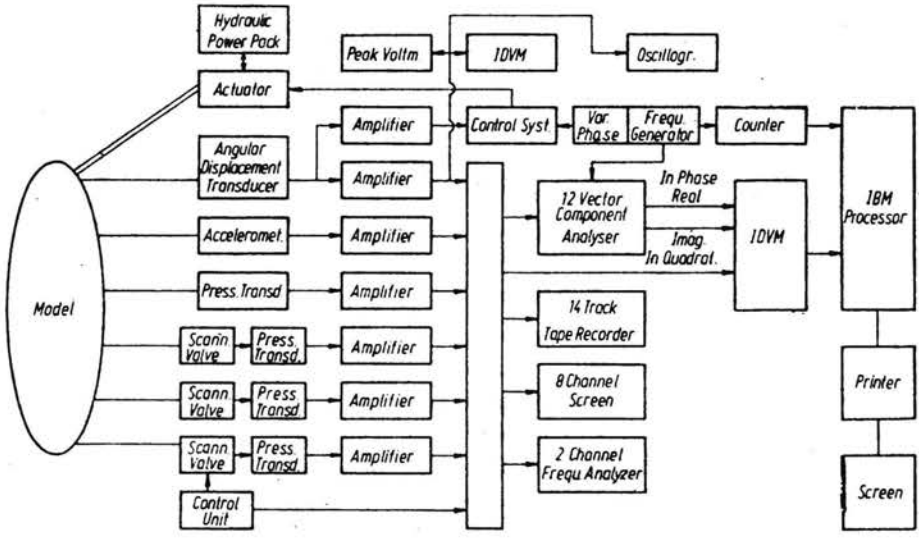

FIG. 4. Block diagram of the measuring equipment.

were measured by a calibration process which was carried out before the wind tunnel test. In addition to the pressure tube system, some few in situ transducers were installed in special positions in order to receive a direct pressure signal comparable with the calibrated pressures obtained by the tubes.

For all the pressure measuring positions the time averaged as well as the unsteady pressures (real and imaginary parts) were measured. For the in situ transducers the whole time-dependent signals were recorded on a tape for later investigation of the corresponding frequency spectrum.

An on-line data reduction procedure assisted the experiment by showing the final measured results during the tests on a screen.

The varied parameters of the experiment were the oscillation frequency, the angle of attack and the wind tunnel speed.

4. Results

4.1. Comparison of theory with experimental results

In Figs. 5–8 experimental data are compared with theoretical results for various angles of incidence from $\alpha_s = 0°$ up to $\alpha_s = 30°$. The three plots in each figure show the steady

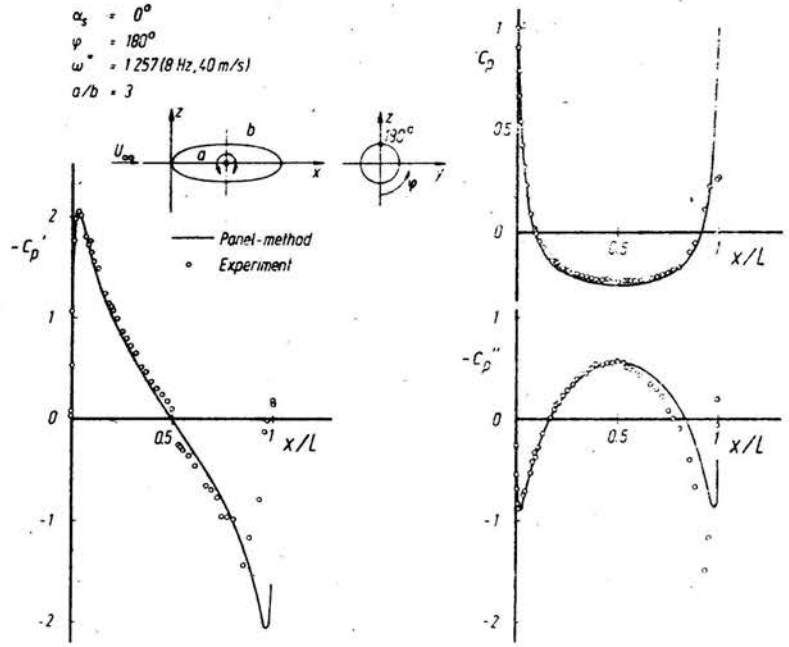

FIG. 5. Ellipsoid with pitching oscillations. Comparison between theory and experiment $\alpha_s = 0°$.

pressures (c_p) as well as the real (c_p') and imaginary (c_p'') parts of the unsteady pressures, respectively.

Figure 5 shows the results for the case $\alpha_s = 0°$. For the steady pressures the agreement between theory and experiment is very good up to 95% chord where separation effects lead to deviations. Only small differences within the remaining part of the body must be referred to boundary layer displacement effects. An excellent agreement can also be

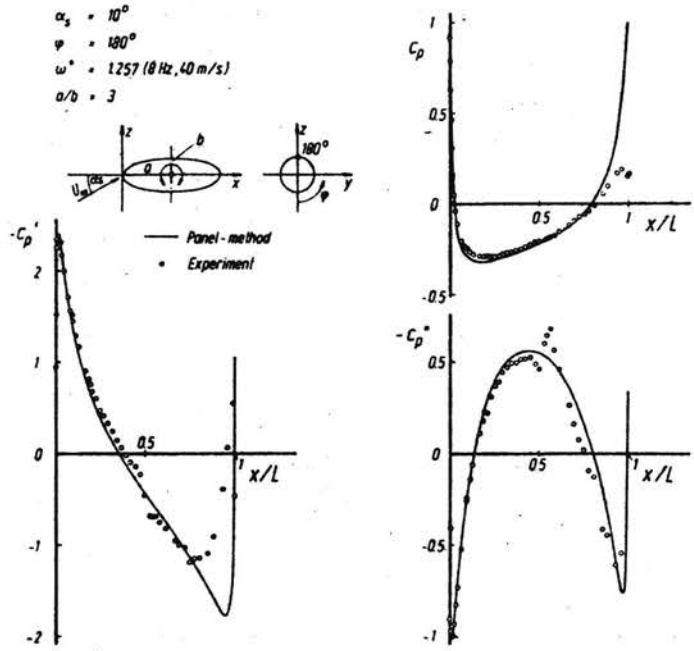

FIG. 6. Ellipsoid with pitching oscillations. Comparison between theory and experiment $\alpha_s = 10°$.

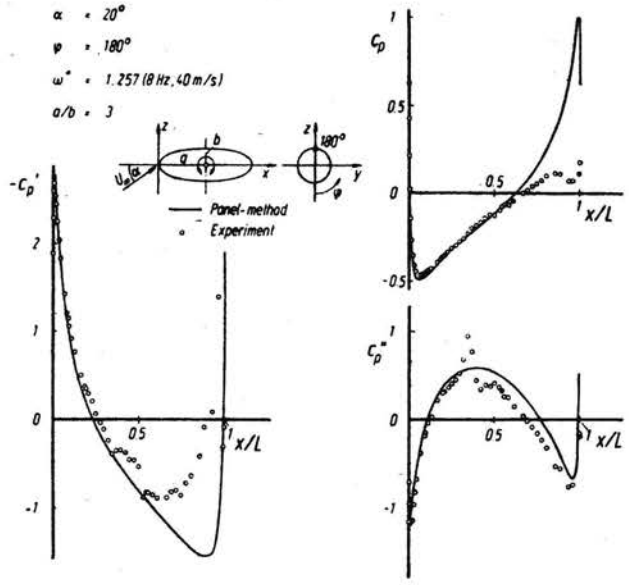

FIG. 7. Ellipsoid with pitching oscillations. Comparison between theory and experiment $\alpha_s = 20°$.

observed for the unsteady pressures within the front part of the body. This agreement is especially remarkable in the region of the sharp pressure peaks.

But on the other hand the plots show clearly the limits of potential theory: A deviation between measured and calculated results occurs quite earlier than in the steady case. It should

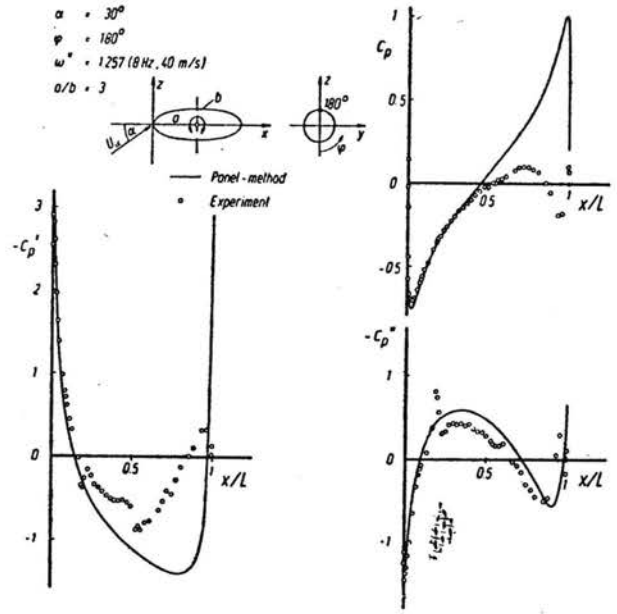

FIG. 8. Ellipsoid with pitching oscillations. Comparison between theory and experiment, $\alpha_3 = 30°$.

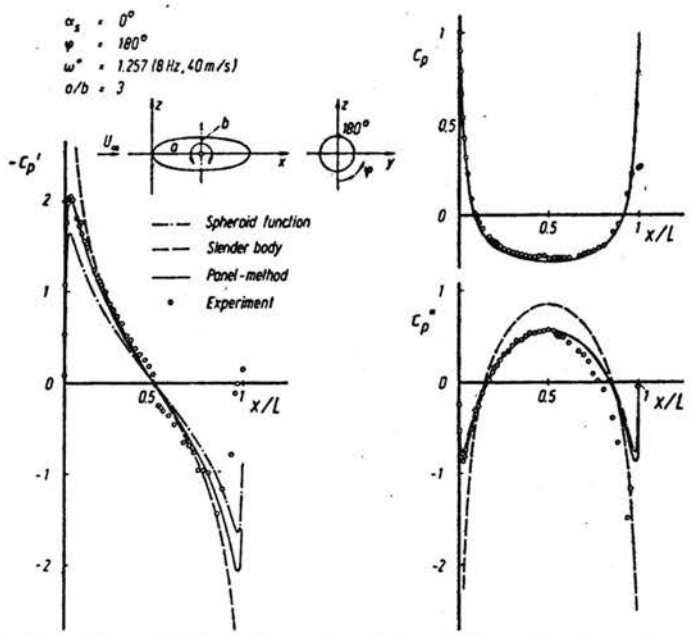

FIG. 9. Ellipsoid with pitching oscillations. Comparison between different theories and experiment, $\alpha_3 = 0°$.

be pointed out that the jumps in the experimental data at $x/L = 0.5$ must be referred to the small irregularity on the body surface due to the body division line at this point.

Figure 6 gives the results for $\alpha_s = 10°$. Again there is excellent agreement between theory and experiment for both steady and unsteady pressure distributions. But deviations which must be referred to viscosity effects are shifted forward to smaller chordwise positions. These tendencies are even more obvious for the cases with higher incidence $\alpha_s = 20°$ (Fig. 7) and $\alpha_s = 30°$ (Fig. 8). Remarkable is the increasing deviation of the measured imaginary parts c_p'' from the theoretical curve. One can observe a peak in c_p'' which is shifted forward with increasing incidence. This peak must obviously be referred to separation effects which occur on such bodies at incidence in the form of free vortex layers [3]. These layers have the tendency to roll up forming a pair of contra rotating body vortices well-known from wind tunnel flow visualizations and calculations.

Summarizing, one should point out that the present theoretical approach fits very well with the experimental results as long as the flow is unseparated. In Fig. 9 the well-known slender body theory and a new method based on the application of spheroid functions [1] are compared with the results of the panel method and with experimental data for the case of zero incidence: both additional approaches show larger deviations at the front part of the body with the well-known singular behavior of the simple slender body theory in this region.

4.2. Additional results

For a further investigation of the pressure peaks in the plots of the imaginary parts (Figs. 5–8), the unsteady pressures are given in Fig. 10 by their magnitude distributions and phase angles. The magnitude distributions show a peak, whereas the phase angles are

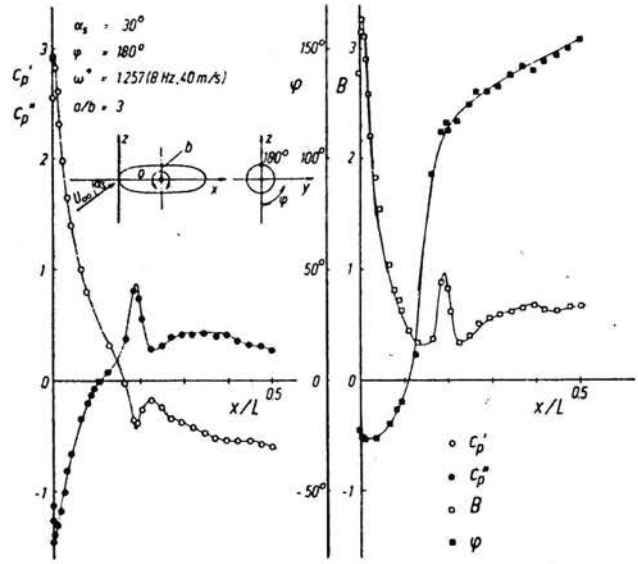

FIG. 10. Ellipsoid with pitching oscillations. Real and imaginary parts of the unsteady pressures compared with their magnitude distributions and phase angles $\alpha_s = 30°$.

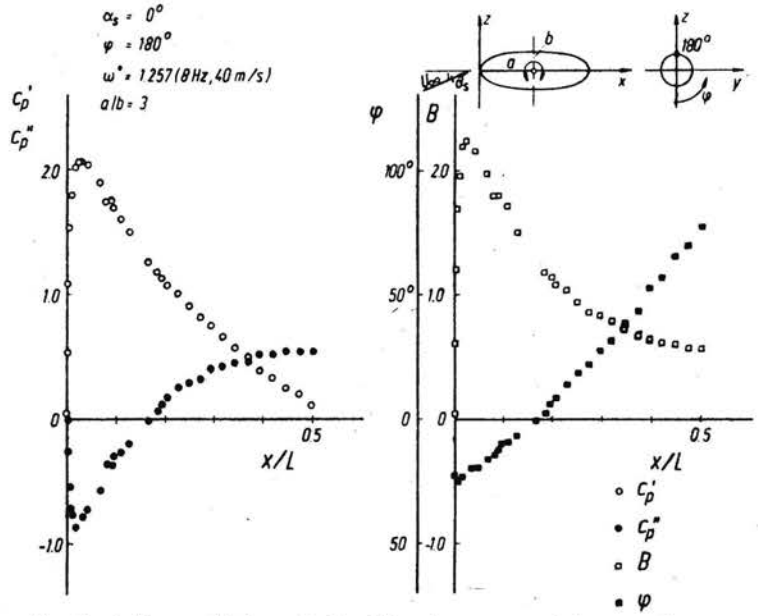

FIG. 11. Ellipsoid with pitching oscillations. Real and imaginary parts of the unsteady pressures compared with their magnitude distributions and phase angles $\alpha_s = 0°$.

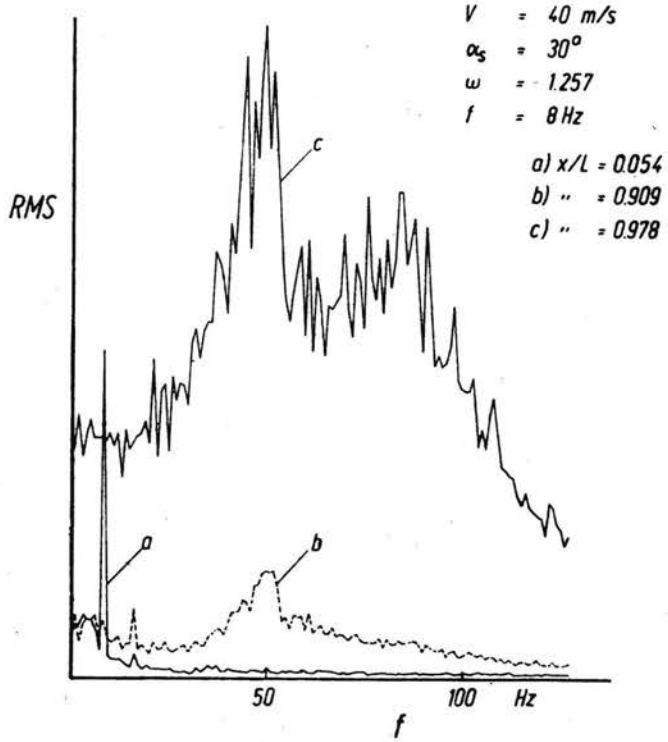

FIG. 12. Power spectra at different positions of the ellipsoid $\alpha_s = 30°$.

discontinous at the previously-mentioned separation region of the free vortex layer type. Further investigations must be carried out in order to clear the character of these phenomena. In Fig. 11 magnitude and phase-angles are plotted for the zero incidence case and no discontinuities can be observed.

Figure 12 shows frequency spectra of the pressures within three different positions of the body measured by in situ pressure transducers. In the most downstream position $x/L = 0.978$, the flow is obviously fully separated and a broad spectrum of pressure fluctuations can be observed within this point. It is noteworthy to mention that a comparison of the measured first harmonics of the pressure with potential theory has not much sense in this separated region of the body.

Within the broad frequency spectrum at $x/L = 0.978$ of Fig. 12, no definite first harmonic pressure peak can be observed. Thus the experimental method as well as the theoretical approach do not take into account the real physics of the separated flow.

5. Summary

Theoretical and experimental investigations of the steady and unsteady airloads on an oscillating ellipsoid of axis ratio $a/b = 3$ have been carried out. The main parameters of this investigation were the mean angle of incidence, the frequency and the wind tunnel speed. The results show an excellent agreement between theory and experiment as long as viscous effects do not play a dominant role. Without incidence only the quasi-two-dimensional separation can be observed at the rear part of the rather blunt body. With increasing incidence an additional phenomenon at the front part of the body is observed which must also be referred to a special type of separation. For a detailed interpretation of the latter problem, further investigations must be carried out. Several results and conclusions can be drawn by the present investigation:

1. The comparison of a sophisticated potential theoretical approach and carefully measured experimental data gives detailed insight into the effects of viscosity.

2. The experimental results of unsteady surface pressures are very sensitive with respect to flow separation.

3. The present investigation shows the problems which must be investigated in the future.

References

1. K. L. CHAO, *Analytische Lösung der verallgemeinerten Helmholtz-Wellengleichung für kompressible Unter-schallströmung und Berechnung der instationären Druckverteilungen an harmonisch schwingenden rotationselliptischen Körpern*, DLR-FB, 77–11, 1977.
2. W. GEISSLER, *Berechnung der Druckverteilung an harmonisch oszillierenden dicken Rümpfen in inkompressibler Strömung*, DLR-FB, 76–48, 1976.
3. W. GEISSLER, *Three-dimensional laminar boundary layer over a body of revolution at incidence and with separation*, AJAA J., **12**, 12, 1743–1745, December 1974.

DFVLR-INSTITUT FÜR AEROELASTIK, GÖTTINGEN, FRG.

Received October 25, 1979.